Low-energy Signals from Supersymmetry

Andries van der Schaaf
Physik-Institut der Universität Zürich
vanderschaaf@psi.ch

Low-energy constraints on supersymmetry are reviewed, with emphasise on R-parity violating processes, in particular those violating L or L_i.

1 Introduction

With the possible exception of finite neutrino masses all present observations in particle physics are consistent with the predictions of the minimal Standard Model. Still, many open questions remain and there is a general believe that the model should be looked at as a highly successful low-energy approximation of some more fundamental theory.

One of the most promising candidates for such a theory beyond the Standard Model is Supersymmetry between bosons and fermions [1]. All known particles are assumed to have "superpartners" differing by half a unit of spin. All non-Lorentzian quantum numbers are identical within one supermultiplet. Although many of us get nervous by this doubling of the number of particle states, one should keep in mind that this situation has occurred more than once before for the fermionic fields (see Fig. 1) when the concepts of helicity, anti-particles and generation were introduced. In the supersymmetric limit

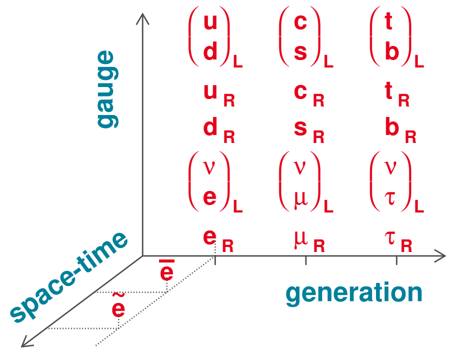

Figure 1: In supersymmetry all fundamental matter fields get bosonic partners denoted by a tilde.

masses and couplings are identical and it can be shown that loop corrections to the boson masses are finite, contrary to the situation in the Standard Model. Although observation tells us that supersymmetry would be a hidden symmetry the symmetry breaking can be achieved "softly", i.e. such that the loop-corrections remain finite (see below). This nice property requires that the superparticles have masses not too far above m_W, i.e. below $\approx$1 TeV, which means that the predicted new forms of matter should become observable within the coming decade, either through direct observation at the high-energy frontier, or through virtual effects in low-energy precision measurements.

In Part I our present knowledge about masses and couplings of supersymmetric particles is reviewed. A separate section is devoted to the interplay of supersymmetry and grand-unification, which could lead to observable rates for lepton-flavor violating particle decays. In Part II future experimental searches for such processes are presented.

Part I
Present constraints on SUSY parameters

2 The Superpotential

The SUSY Lagrangian is described in terms of the superpotential:

$$\begin{aligned} W &= h_l^{ij} E_i^c L_j H_d + h_d^{ij} Q_i D_j^c H_d + h_u^{ij} Q_i U_j H_u + \mu H_u H_d + \\ &\quad + \frac{1}{2}\lambda_{ijk} L_i L_j E_k^c + \lambda'_{ijk} L_i Q_j D_k^c + \frac{1}{2}\lambda''_{ijk} U_i^c D_j^c D_k^c \end{aligned} \tag{1}$$

with:

i, j and k : generation indices
Q and L : doublet superfields
U^c, D^c and E^c : singlet superfields

The trilinear couplings λ_{ijk} , λ'_{ijk} and λ''_{ijk} violate R-parity, which is even for particles and odd for superparticles [2]:

$$R_p = (-1)^{3(B-L)+2S} \tag{2}$$

B : baryon number
L : lepton number
S : spin

λ_{ijk} and λ''_{ijk} are anti-symmetric ($\lambda_{ijk} = -\lambda_{jik}$ and $\lambda''_{ijk} = -\lambda''_{ikj}$) resulting in 3^2=9 complex parameters each. λ''_{ijk} gives additional 3^3=27 parameters.

3 Explicit R-parity violation

The R_p violating terms in the superpotential (Eq.1) would lead to corrections to the standard model predictions of a large number of experimental quantities. Since no such deviations have been found, the measurements result in upper limits on the values of the λ_{ijk}, λ'_{ijk} and λ''_{ijk} couplings.

The constraints may be separated into constraints on single operators, which do not depend on the values of any of the other couplings, and constraints on the product of two operators. They have been calculated assuming a generic SUSY mass of 100 GeV. For larger values the bounds are weakened correspondingly. See [5] for a recent review.

3.1 single operators

Examples of quantities that constrain single λ couplings are:

- The **neutrino Majorana mass** m_{ν_e} receives contributions from fermion-sfermion loops. The corresponding coupling amounts to:

$$\lambda \approx \frac{2\pi}{m_f}\sqrt{\frac{2m_{\nu_e}\tilde{m}}{N_c}} \tag{3}$$

  Assuming m_{ν_e} < 5eV from the direct determinations from tritium decay, this corresponds to λ_{133} <0.003 from the contribution from the $\tau\tilde{\tau}$ loop (N$_c$=1) and λ'_{133} <0.0007 from the $b\tilde{b}$ loop (N$_c$=3).

- **Neutrinoless double beta decay** gives very severe constraints on both single and product Yukawa's. An upper limit

$$\lambda'_{111} \approx 10^{-3}\sqrt{\frac{t_{1/2}}{10^{25}y}} \tag{4}$$

  has been obtained [3], scaled to the present experimental limit $t_{1/2}^{0\nu\beta\beta}(^{76}\mathrm{Ge}) > 10^{25}$ y.

- V_{ud} would be modified as follows:

$$|V_{ud}^{exp}|^2 = |V_{ud}^{SM}|^2[1 + 2r'_{11k}(\tilde{d}_R^k)/V_{ud} - 2r_{12k}(\tilde{e}_R^k)], \tag{5}$$

  with $r_{ijk}(\tilde{l}) \equiv (M_W^2/g^2)(\lambda_{ijk}^2/m_{\tilde{l}}^2)$

- **Charged-lepton universality** would be modified:

$$R_\pi = R_\pi^{SM}[1 + \frac{2}{V_{ud}}(r'_{11k}(\tilde{d}_R^k) - r'_{21k}(\tilde{d}_R^k))], \tag{6}$$

  with $R_\pi \equiv \Gamma(\pi \to e\nu)/\Gamma(\pi \to \mu\nu)$

- The perfect agreement of the weak charge Q_W observed in measurements of **atomic parity violation** (Q_W^{exp}=-72.11±0.93 compared to Q_W^{SM}=-73.17±0.13) leads to constraints on a number of couplings, which are incompatible with R violation interpretation of former high Q^2 HERA anomaly [4]. This example shows the usefulness of this type of phenomenological analysis, which allows the comparison of observations from two wildly different energy domains.

Table 1: Upper limits on R_p violating couplings from single operators, calculated for $\tilde{m}$=100 GeV (from [5]).

λ_{ijk}			λ'_{ijk}									λ''_{ijk}		
121	131	231	111	121	131	211	221	231	311	321	331	112	113	123
122	132	232	112	122	132	211	222	232	312	322	332	212	213	223
123	133	233	113	123	133	211	223	233	313	323	333	312	313	323
5%	6%	6%	0.1%	4%	4%	9%	18%	22%	16%	20%	26%	10^{-6}	10^{-5}	
5%	6%	6%	2%	6%	33%	9%	18%	39%	16%	20%	26%			
5%	0.4%	6%	2%	20%	0.2%	9%	18%	39%	16%	20%	26%	43%	43%	43%

The limits deduced from these observables, as well as $D^o - \overline{D}^o$ mixing, ν_μ deeply inelastic scattering, B($\tau \to \pi\nu$), heavy nucleon decay, $n - \overline{n}$ oscillations and the branching ratios $\Gamma(\tau \to e\nu)/\Gamma(\tau \to \mu\nu)$, $\Gamma(Z^o \to \text{hadrons})/\Gamma(Z^o \to \text{leptons})$ and $\Gamma(D^+ \to \overline{K}^o \mu^+\nu)/\Gamma(D^+ \to \overline{K}^o e^+\nu)$, are summarized in Table 1.

Taking into account the uncertainties in $\tilde{m}$, one should conclude that only the limits on λ''_{112} and λ''_{113} are unnaturally low. Even better limits on these couplings come from product operators, discussed below, which are constrained by the observed proton stability.

3.2 product operators

The most sensitive tests of R_p conservation come from processes involving $\Delta L_i \neq 0$, $\Delta B \neq 0$ or tree-level $\Delta S = 2$ operators. Some examples are shown in Fig. 2. Table 2 lists

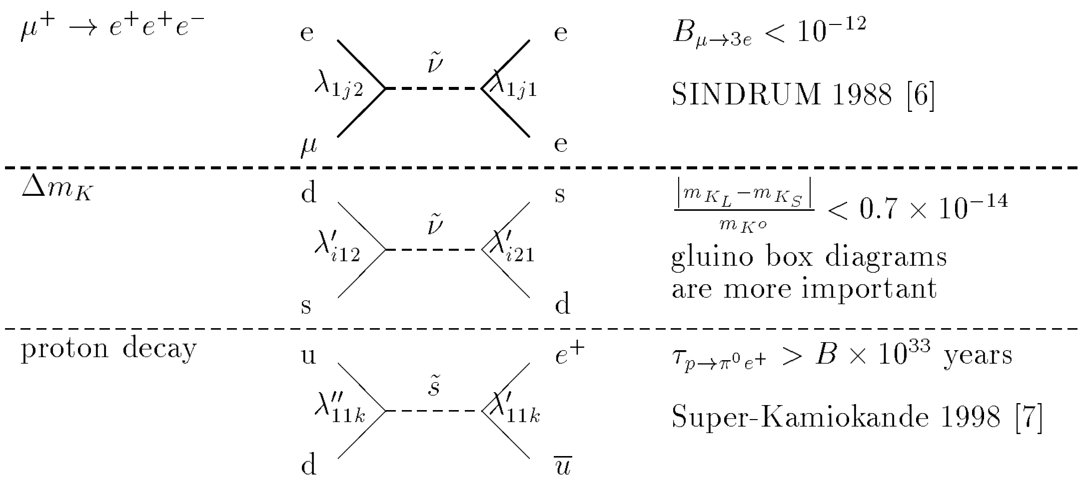

Figure 2: R_p violating processes requiring two finite couplings.

the most severe constraints on $\lambda_{ijk}.\lambda_{ijk}$, $\lambda'_{ijk}.\lambda'_{ijk}$ and $\lambda'_{ijk}.\lambda''_{ijk}$ products. As noticed above already, the limits on λ''_{ijk} couplings, deduced from proton stability, are so low that one should assume $\lambda''_{ijk} \equiv 0$. In the following we will assume $\lambda_{ijk}=\lambda'_{ijk}=\lambda''_{ijk}=0$, i.e. no explicit R_p violation.

Table 2: Products of R_p violating couplings.

	$\lambda_{ijk}.\lambda_{ijk}$	
$\mu^+ \to e^+e^+e^-$	$\lambda_{ijk1j1}\lambda_{ijk1j2}$ $< 7 \times 10^{-7}$	$\lambda_{ijk231}\lambda_{ijk131}$ $< 7 \times 10^{-7}$
	$\lambda'_{ijk}.\lambda'_{ijk}$	
$K \to \mu e$	$\lambda'_{ijk1j1}\lambda'_{ijk2j2}$ $< 8 \times 10^{-7}$	
Δm_K	$\lambda'_{ijki12}\lambda'_{ijki21}$ $< 10^{-9}$	
Δm_B	$\lambda'_{ijki13}\lambda'_{ijki31}$ $< 3 \times 10^{-8}$	
$(2\beta)_{0\nu}$	$\lambda'_{ijk113}\lambda'_{ijk131}$ $< 3 \times 10^{-8}$	
$\mu^-(A,Z) \to e^-(A,Z)$	$\lambda'_{ijk1j1}\lambda'_{ijk2j1}$ $< 5 \times 10^{-8}$	$\lambda'_{ijk11k}\lambda'_{ijk21k}$ $< 5 \times 10^{-8}$
	$\lambda'_{ijk}.\lambda''_{ijk}$	
proton lifetime	$\lambda'_{ijk11k}\lambda''_{ijk11k}$ $< 10^{-27}$	$\lambda'_{ijkijk}\lambda''_{ijklmn}$ $< 10^{-11}$

4 Minimal Supersymmetry

Without explicit R_p violation the superpotential (Eq. 1) reduces to:

$$W = h_l^{ij} E_i^c L_j H_d + h_d^{ij} Q_i D_j^c H_d + h_u^{ij} Q_i U_j H_u + \mu H_u H_d \tag{7}$$

Proportionality further reduces the superpotential of Eq. 7 to:

$$W = h_l^i E_i^c L_i H_d + h_d^i Q_i D_i^c H_d + V_{CKM}^{ji} h_u^j Q_i U_j H_u \tag{8}$$

The superpotential (Eq. 8) conserves lepton flavor. A remaining source of flavor dependence is found in the terms responsible for **SUSY breaking**.

In the SUSY limit the superpotential is not affected by higher orders in perturbation theory. SUSY breaking may be achieved, keeping corrections to m_W and m_H finite, by **soft-breaking terms**:

- Gaugino mass terms (gluino, wino, bino)
- Sfermion mass terms
- bi-linear and tri-linear couplings

The number of parameters is reduced by the assumption of **universality**: these terms are flavor-independent at some high fundamental mass scale. In most models the SUSY-breaking interaction (i.e. gravity) is flavor-blind as well, which guarantees that the renormalization of masses and couplings down to the electroweak scale does not affect the conservation of lepton-flavor.

5 Bounds from electroweak precision tests

Electroweak precision data agree perfectly with the standard model predictions and it is interesting to see what region of SUSY parameter space can be excluded from these data. To lowest order any electroweak process only depends on:

- fine structure constant: $\alpha = 137.0359895(61)^{-1}$
- Fermi constant: $G_F = 1.16639(2)10^{-5}$ GeV^{-2}
- mass of Z boson: $M_Z = 91.1867(20)$ GeV

Higher-order corrections require the knowledge of:

- the fermion masses, in particular: $m_{top} = 175.6 \pm 5.5$ GeV
entering as $(m_f/m_Z)^2$
- Higgs mass: a free parameter between 77 GeV and ≈1 TeV
enters as $\ln(m_H/m_Z)$
- the strong coupling constant: $\alpha_s = 0.118 \pm 0.003$
enters in gluon radiative corrections

Figure 3 shows as an example how the top quark contributes to the decay $Z \to b\bar{b}$.

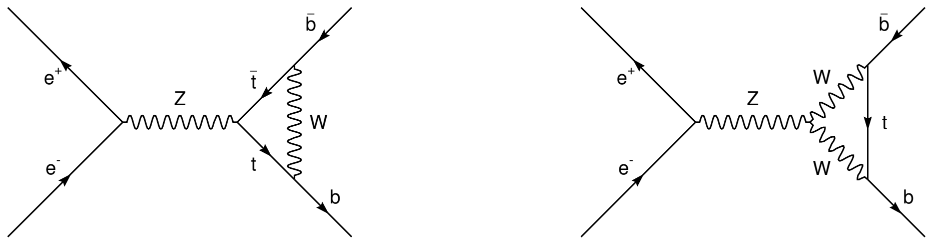

Figure 3: Diagrams for vertex correction to $Z \to b\bar{b}$ involving the top quark. These contributions do not decrease, but increase with the fermion mass and are of order $\mathcal{O}(1\%)$.

As a result any electroweak observable can be computed as: $O_i(\alpha, G_F, m_Z, m_f, m_H, \alpha_s)$. The Higgs mass can thus be determined from a fit to the data. Table 3 shows the sensitivity of R_b, $\sin^2\theta$, R_l and α_s to variations in m_{top} and m_H.

Table 3: Sensitivity of four electroweak observables to m_{top} and m_H. Reference value for the Higgs mass is 300 GeV. Intrinsic uncertainties are ≈0.02% (from [8]).

O_i	σ_{exp}	m_{top} ±6 GeV	m_H=70 GeV	m_H=1 TeV
Γ_Z	0.1%	±0.06%	0.17%	-0.21%
R_l	0.1%	-	0.07%	-0.06%
R_b	0.4%	±0.09%	-0.02%	0.00%
$\sin^2\theta$	0.1%	±0.08%	-0.4%	0.3%

Erler and Pierce [9] have performed global fits to the 31 electroweak observables shown in Table 4. The fit gives χ^2=26.6 for 26 degrees of freedom and results in $m_H = 109^{+108}_{-60}$ GeV. If treated as a free parameter m_{top} is predicted 181±18 GeV as compared to the measured value of 175±6 GeV.

Table 4: Experimental values of 31 electroweak observables and the result of a global standard-model fit to these data (from [9]).

observable	measurement	SM fit	pull
M_Z (GeV)	911867(20)	911867	0.0
Γ_Z (GeV)	24949(25)	24959	-0.4
M_W (GeV)	80430(76)	80386	0.6
m_t (GeV)	175(5)	172	0.6
σ_{had} (nb)	41486(53)	41478	0.2
$\Gamma_{\mathrm{had}}/\Gamma_e$	20575(56)	20744	0.2
$\Gamma_{\mathrm{had}}/\Gamma_\mu$	20583(37)	20744	1.1
$\Gamma_{\mathrm{had}}/\Gamma_\tau$	20823(50)	20744	0.7
$\Gamma_b/\Gamma_{\mathrm{had}}$	02170(9)	02158	1.3
$\Gamma_c/\Gamma_{\mathrm{had}}$	01734(48)	01722	0.2
A_e^{FB}	00160(24)	00163	-0.1
A_μ^{FB}	00163(14)	00163	0.0
A_τ^{FB}	00192(18)	00163	1.6
A_e	01548(33)	01476	2.2
A_μ^{FBLR}	0102(34)	0148	-1.3
A_τ^{FBLR}	0195(34)	0148	1.4
A_b^{FB}	00984(24)	01035	-2.1
A_c^{FB}	00741(48)	00739	0.0
A_b^{FBLR}	0900(50)	0935	-0.7
A_c^{FBLR}	0650(58)	0668	-0.3
P_τ	01411(64)	01476	-1.0
P_τ^{FB}	01399(73)	01476	-1.1
$\sin^2\theta_{\mathrm{eff}}$	02322(10)	02315	0.8
Q_W(Cs)	-7211(93)	-7311	1.1
Q_W(Tl)	-1148(3.7)	-1167	1.1
κ(DIS)	0581(4)	0583	-0.7
$\mathrm{g}_V^{\nu e}$	-0041(15)	-00396	-0.1
$\mathrm{g}_A^{\nu e}$	-0507(14)	-0506	-0.0
$\log(B_{B\to X_s\gamma})$	-849(45)	-799	-1.1
$\Delta\alpha_{\mathrm{had}}^{(5)}$	002817(62)	002817	0.0
$\alpha_s(M_Z)$	0118(3)	01195	-0.5

One-loop supersymmetric corrections have been included in two SUSY-breaking scenarios, described by the following parameters:

minimal supergravity (SUGRA)	
scalar mass	M_o
gaugino mass	$M_{1/2}$
tri-linear coupling	A_0
Higgs vev ratio	$\tan\beta$
Higgsino mass parameter	μ

minimal gauge-mediated model (GM)	
scale parameter	Λ
Higgs vev ratio	$\tan\beta$
Higgsino mass parameter	μ

For large SUSY masses ($>> M_Z$) the electroweak data data are not sensitive. For low SUSY masses the fit generally gets worse, which results in lower limits on the various mass parameters (see Table 5). One should conclude that evidence for SUSY should come from other sources.

Table 5: Lower limits on SUSY masses in GeV (from [9]).

	SUGRA		GM_5		GM_{10}	
sgn(μ)	+	-	+	-	+	-
μ	135	-135	200	-200	180	-165
M_0	9	0	-	-	-	-
$M_{1/2}$	105	120	-	-	-	-
Λ (TeV)	-	-	36	41	14	13
$\tan\beta_{min}$	1.4	1.2	1.3	1.2	1.3	1.2
$\tan\beta_{max}$	36	60	45	65	39	52
m_h	78	78	78	78	78	78
m_H,m_A	320	115	255	220	230	185
m_{H+}	330	140	265	235	240	205
$m_{\tilde{e}_R}$	74	66	73	76	70	63
$m_{\tilde{e}_L}$	105	110	140	150	125	120
$m_{\tilde{\tau}_1}$	53	48	73	55	70	52
$m_{\tilde{\tau}_2}$	110	110	140	150	125	120
$m_{\tilde{u}_L}$	285	295	355	405	355	335
$m_{\tilde{u}_R}$	280	290	330	375	340	325
$m_{\tilde{d}_L}$	295	305	360	410	360	345
$m_{\tilde{d}_R}$	285	290	325	370	335	325
$m_{\tilde{t}_1}$	56	66	275	170	290	175
$m_{\tilde{t}_2}$	275	310	355	420	365	385
$m_{\tilde{b}_1}$	185	250	320	345	330	310
$m_{\tilde{b}_2}$	285	295	325	370	335	330

6 Supersymmetric Grand-unification

The assumed universality of squark and slepton masses in minimal SUSY leads to the absence of tree-level FCNC and lepton-flavor violation in particular. As discussed first by Hall, Kostelecky and Raby [10] in unified theories flavor-violation is introduced by loop corrections above the unification scale. It was realized later [11] that the large flavor-violation observed in the top-Yukawa coupling leads to measurable rates for L_i violating processes, in particular the decay $\mu \to e\gamma$, even in standard SUSY SU(5). Figure 4,

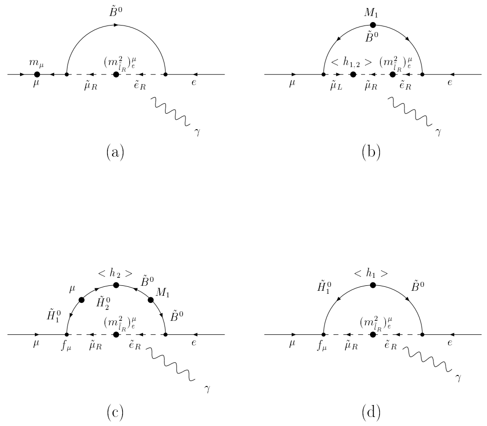

Figure 4: Feynman diagrams contributing to the decay $\mu \to e\gamma$ in the minimal SUSY SU(5) GUT (from [12]).

taken from [12] shows $\mu \to e\gamma$ diagrams in minimal SUSY SU(5). All contributions are proportional to $(m^2_{\tilde{l}_R})^\mu_e$, which in turn depends strongly on the top mass (see Fig. 5).

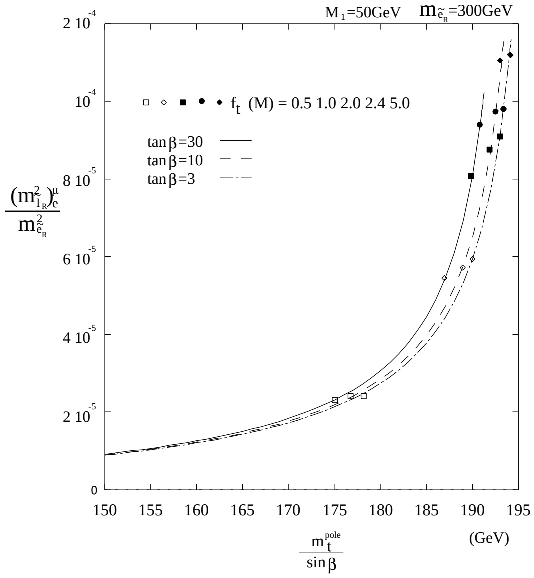

Figure 5: μe mixing matrix element at the electroweak scale versus top mass.

Since both amplitude ratios A_a/A_d and A_b/A_c (subscript corresponds to the four diagrams of Fig. 4) are negative cancellations may give a large reduction of $B_{\mu\to e\gamma}$ as illustrated in Fig. 6. Fortunately, the cancellations differ for the various L_i violating processes

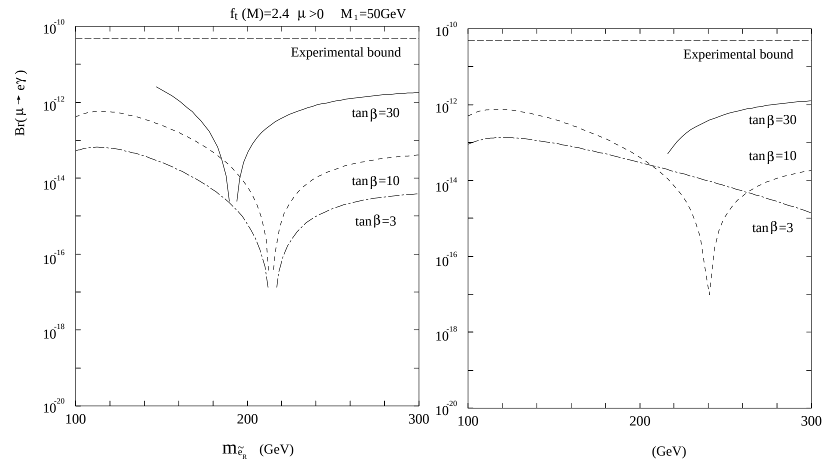

Figure 6: Predictions for the $\mu \to e\gamma$ branching ratio (from [12]).

and can not lead to a significant suppression of all modes simultaneously. For this reason different tests are performed, as discussed in Part II.

Part II

Experimental tests of L and L_i violation

7 Neutrinoless double beta decay $(2\beta)_{0\nu}$

Neutrinoless double beta decay offers a very sensitive test of the conservation of total lepton number.

7.1 Status

Figure 7 shows the results of the various searches and the expectations for the improvements in the years to come. The observed lower limit on the lifetime is usually translated into an upper limit of the Majorana neutrino mass. There are, however, several alternative mechanisms for the process, i.e. R_p violating supersymmetry (see Part I). The best limit so-far was reached for ^{76}Ge by the Heidelberg-Moscow experiment, based

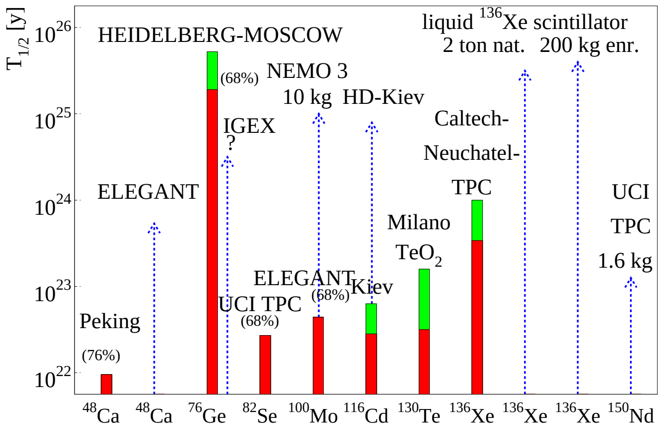

Figure 7: Experimental limits on neutrinoless double beta decay. Dark bars: present limits, grey bars: sensitivities expected in the next few years, arrows: future prospects.

in the Gran Sasso underground laboratory. This experiment is presently taking data with five high-purity Ge detectors, enriched to 86% ^{76}Ge, with a total mass of 11 kg. Fig. 8

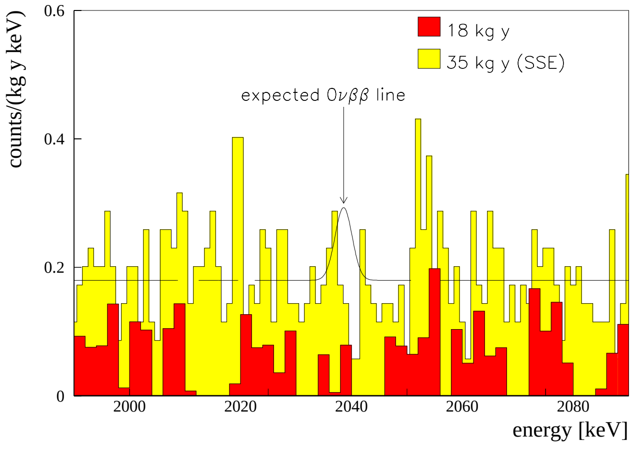

Figure 8: Energy spectrum.

shows the energy spectrum, accumulated during the past 3 years. For ≈ 50% of the data a pulse-shape analysis reduced the background from 0.2 to 0.07 counts per kg.y.keV. It is clear from Fig. 8 that no signal is found, which corresponds to:

$$T_{1/2} > 1.2 \cdot 10^{25} y \;, \tag{9}$$

corresponding to an upper limit of 0.44 eV for the Majorana ν mass. The group plans to continue data-taking until 2003.

7.2 GENIUS

The Heidelberg-Moscow collaboration intends to upgrade their experiment to 288 enriched ^{76}Ge crystals (total weight 1 ton), positioned in a large tank filled with liquid nitrogen for cooling and shielding. Simulation shows that background should be under control (see Fig.9). With this setup the sensitivity could be improved by almost three orders of

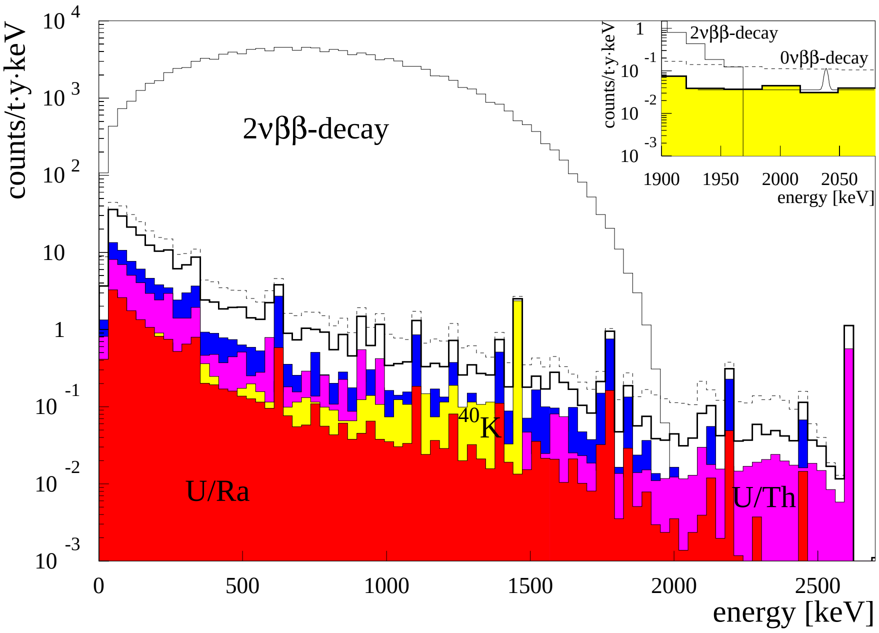

Figure 9: Result of a simulation of the background in the proposed GENIUS experiment, taking into account various contaminations in the liquid nitrogen. Dashed line: total background. Solid line: background remaining after requiring only single hit crystal.

magnitude compared to the present one, or about a factor 30 in the neutrino mass.

8 Tests of lepton-flavor violation

Although various anomalies in the fluxes of solar, atmospheric and beam dump neutrinos may be interpreted in terms of neutrino oscillations, no convincing signal for the violation of lepton-flavor violation has been observed so far. Searches for LFC-violating decay modes of charged leptons, mesons and Z^0 have resulted in upper limits only, as summarized in Table 6. Since the experimental sensitivities are mostly limited by the available beam intensities or luminosities the most stringent limits come from μ and K decays. The best limits have thus been obtained for transitions between the lighter two generations. In models, in which the couplings involving the third] generation are strongly enhanced, the constraints from Z, τ and B decays start to become interesting too.

Table 6: Branching ratios of some LFC-violating decay modes.

Decay mode	Branch. Ratio
$\mu^+ \to e^+\gamma$	$< 4.9 \times 10^{-11}$
$\to e^+e^+e^-$	$< 1.0 \times 10^{-12}$
$\mu^- S \to e^- S$	$< 7 \times 10^{-11}$
$\mu^- Ti \to e^- Ti$	$< 6.1 \times 10^{-13}$
$\to e^+ Ca^*$	$< 3.6 \times 10^{-11}$
$\mu^- Pb \to e^- Pb$	$< 4.6 \times 10^{-11}$
$\mu^+ e^- \leftrightarrow \mu^- e^+$	$< 8.2 \times 10^{-11}$
$\tau \to e\gamma$	$< 2.7 \times 10^{-6}$
$\tau \to \mu\gamma$	$< 3.0 \times 10^{-6}$
$\tau \to 3$ charged leptons	$< 3 \times 10^{-6}$
$K^+ \to \pi^+ \mu e$	$< 2.1 \times 10^{-10}$
$K_L^o \to \mu e$	$< 3.3 \times 10^{-11}$
$B^o \to \mu e$	$< 5.9 \times 10^{-6}$
$\to \tau e$	$< 5.3 \times 10^{-4}$
$\to \tau\mu$	$< 8.3 \times 10^{-4}$
$Z^0 \to e\mu$	$< 1.7 \times 10^{-6}$
$\to e\tau$	$< 9.8 \times 10^{-6}$
$\to \mu\tau$	$< 1.7 \times 10^{-5}$

9 $\mu - e$ conversion

Neutrinoless $\mu^- \to e^-$ conversion in muonic atoms, $\mu^-(A,Z) \to e^-(A,Z)$ with A mass number and Z atomic number, gives the best constraints on LFC violation in a large variety of models. For conversions leaving the nucleus in its ground state the nucleons act coherently, which boosts the conversion probability relative to the rate of the dominant process of nuclear muon capture.

When negative muons stop in matter, they quickly get captured and form muonic atoms, which mostly reach their ground state before decaying by muon decay in orbit

$\mu^-(A,Z) \to e^-\overline{\nu}_e\nu_\mu(A,Z)$ or nuclear muon capture $\mu^-(A,Z) \to \nu_\mu(A,Z-1)$. In the usual convention the branching ratio for $\mu \to e$ conversion is quoted relative to the rate for nuclear muon capture:

$$B_{\mu e} \equiv \frac{\Gamma_{\mu^-(A,Z)\to e^-(A,Z)^{g.s.}}}{\Gamma_{\mu^-(A,Z)\mathrm{capture}}} \,. \tag{10}$$

Assuming LFC violation one may wonder how $B_{\mu e}$ varies as a function of Z and A, and with what probability the nucleus stays in its ground state. Earlier calculations predicted a steady rise of the branching ratio until $Z \approx 30$, from where on it was expected to drop again. For this reason most experiments have been performed on medium-heavy nuclei. More recently it has been estimated that $\mathrm{B}_{\mu e}$ may keep increasing with Z. The same calculations predict the coherent fraction to be larger than 80 % for all nuclear systems.

Experimentally coherent $\mu \to e$ conversion offers a number of advantages. Since the observation of the process requires the detection of only one particle in the final state there are no problems with accidental coincidences, which constitute one of the major limitations in searches for $\mu \to e\gamma$ and $\mu \to 3e$. Since the electron is emitted at the kinematical endpoint ($p_e \approx m_\mu c$) where the rate for the intrinsic background from muon decay in orbit vanishes, the experimental set-up may have a large geometrical acceptance and still the detectors can be protected against the vast majority of decay and capture events.

The signature of coherent $\mu^- \to e^-$ conversion is a monoenergetic electron which is emitted at the kinematical endpoint for bound muon decay, i.e. with an energy equal to the muon mass minus the muon binding energy and the kinetic energy of the recoiling atom:

$$E_{\mu e} = m_\mu c^2 - B(A,Z) - E_{\mathrm{recoil}}(A,Z)\,. \tag{11}$$

In the case of titanium B=1.27 MeV and E_{recoil}=0.12 MeV, which results in $E_{\mu e}$=104.27 MeV.

There are several sources of electron background in the energy region around 100 MeV, involving either beam particles or cosmic rays. Beam-related background may originate from muons, pions or electrons in the beam. Muons may produce background by *muon decay in flight* (MIF) or, after the formation of a muonic atom, by *muon decay in orbit* (MIO) or *radiative muon capture* (RMC). Pions may produce background by *radiative pion capture* (RPC). Capture gammas from RMC and RPC produce electrons mostly through e^+e^- pair production inside the target. Electrons in the beam may produce background through scattering off the target.

The dominant intrinsic background is muon decay in orbit. Energy distributions for MIO electrons have been calculated for a number of muonic atoms [13] and the results are shown in Fig. 10. The spectrum drops steeply above $m_\mu c^2/2$, which is the endpoint energy for free muon decay.

Prompt background can be removed by beam quality, with the help of a beam counter, or by using a pulsed muon beam.

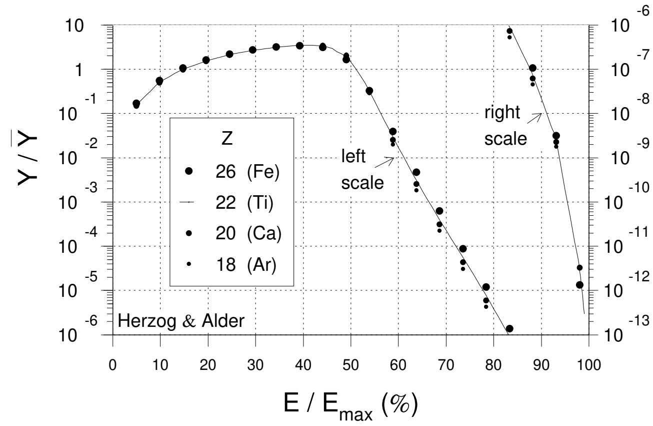

Figure 10: Normalized electron energy distributions from the decay of muonic atoms of Ar, Ca and Fe (from [13]). The titanium spectrum resulted from these distributions by interpolation.

9.1 The SINDRUM II experiment

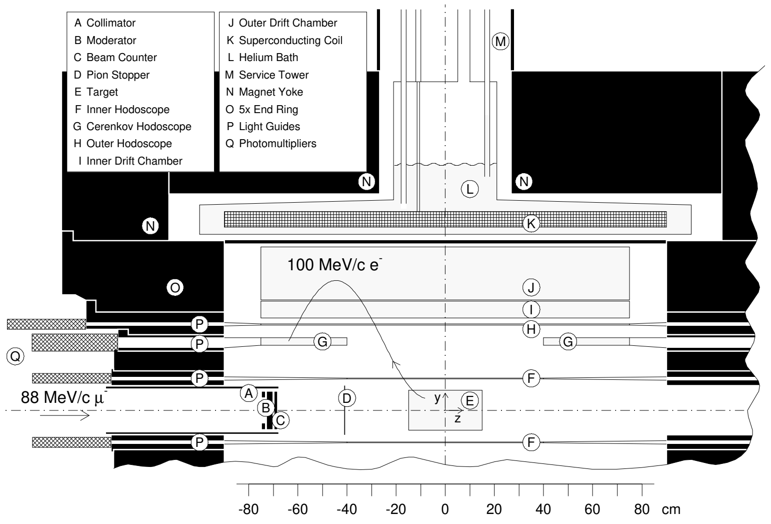

Figure 11: The SINDRUM II spectrometer.

The SINDRUM II experiment aims at a sensitivity of a few times 10^{-14} for $B_{\mu e}$. In a first stage data were taken on titanium and lead at the old μE1 beam line at PSI. The results are listed in Table 6. Here the third and final measurement at this beam is described, a renewed search for $\mu^- \to e^-$ conversion on titanium with a sensitivity below 10^{-12}.

The SINDRUM II spectrometer (see Fig.11) consists of a set of concentric cylindrical detectors inside a superconducting solenoid. The particles of interest follow helical

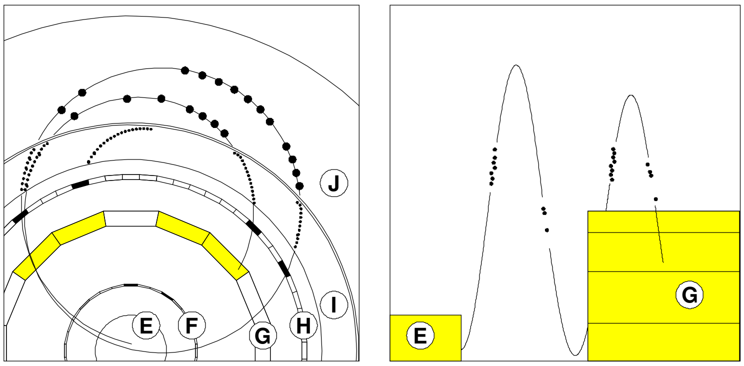

Figure 12: Tracks left in the spectrometer by a 100 MeV/c e^-. The labeling of the detector components is as in Fig. 11.

trajectories, making 1–3 full turns before reaching a Čerenkov hodoscope at either end of the magnet. Two radial drift chambers are used for tracking: (i) DC1, filled with CO_2/iC_4H_{10} (70/30), a slow drift gas with only 6^o Lorentz deflection and (ii) DC2, filled with He/iC_4H_{10} (88/12) for its long 1.14 km radiation length. DC1 gives 3-dimensional space points with the help of cathode strip readout.

Figure 12 shows an example of an electron trajectory making two turns before reaching a Čerenkov hodoscope. The spectrometer performance has been checked by a measurement of the e^+ energy distribution in the decay $\pi^+ \to e^+\nu$. The measured distribution has a FWHM of 1.5 MeV. Figure 13 shows energy distributions for three stages in the event

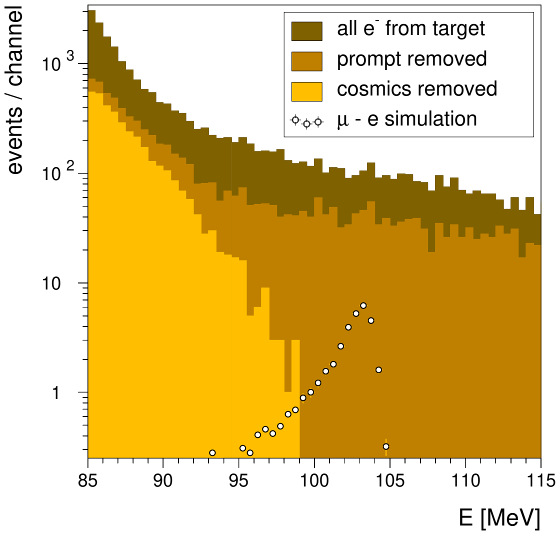

Figure 13: Electron energy distribution at three stages of the event selection and as predicted by a GEANT simulation of $\mu - e$ conversion on titanium assuming $B_{\mu e} = 4 \cdot 10^{-12}$.

selection. The energy distribution of the final sample, which contains 3580 events with an energy above 85 MeV, falls steeply towards zero with an endpoint below 100 MeV. No candidate events have been found corresponding to a 90% C.L. upper limit of 2.3 events. The results are summarized in Table 7.

Table 7: Sensitivity determination and result of the SINDRUM II search for μ-e conversion on titanium.

measuring time	50 days
muon stops	3.1×10^{13}
nuclear capture fraction	85%
geometrical acceptance	42%
total efficiency	35%
1/sensitivity	3.9×10^{12}
sensitivity	2.6×10^{-13}
events seen	¡2.3 (90% C.L.)
90% C.L. upper limit	6.1×10^{-13}

The single-event sensitivity will improve to 10^{-14} next year, when first data will become available at a new beam line. The stop rate is expected to raise to $\approx 10^8$ s^{-1}. Direct beam components will be removed by a combination of collimator and blocker inside a constant magnetic field. Muons form π decays in between pass the blocker with a probability of $\approx$50% .

9.2 The MECO proposal (BNL E940)

This proposal [14], a search for μ-e conversion with a sensitivity below 10^{-16}, is based on the MELC proposal [15] originally planned for the Moscow Meson Factory. In this case prompt background will be removed by beam pulsing. Beam characteristics and resulting sensitivity are listed in Table 8.

Table 8: Sensitivity determination and result of the proposed MECO search.

proton momentum	8 GeV/c	μ captured in Al	5×10^{10}/s
proton intensity	2×10^{13}/s	fraction in Δt window	2×10^{10}/s
burst length	100 ns	reconstructed at B=1	5×10^{9}/s
μs reaching target	2×10^{11}/s	measuring time	10^7 s
μ stops in target	8×10^{10}/s	seen at B=10^{-16}	5

Figure 14 shows the general layout. The tungsten pion production target is placed inside a graded-field solenoid resulting in almost 4π solid angle. Decay muons are transported to the targets through 90^o bend solenoids, giving momentum and charge selection. Electrons from these targets are collected by a second graded solenoid and tracked with low-mass straw drift chambers before reaching a trigger calorimeter.

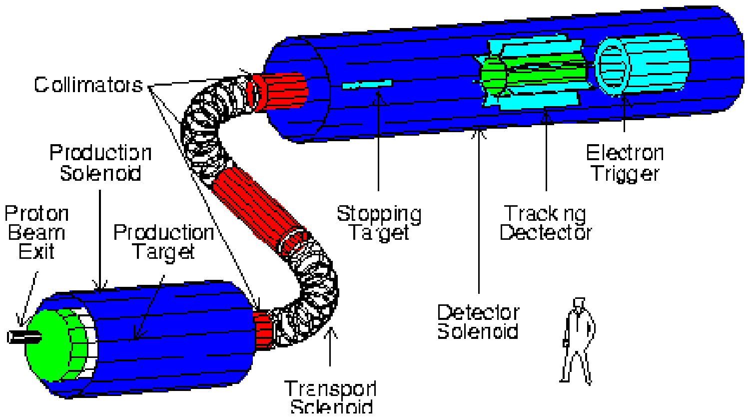

Figure 14: Schematic of the MECO experiment. The magnetic field decreases steadily from 3.3 T at the production target to 1 T at the location of the tracking detector.

10 $\mu \to e\gamma$

At the moment the decay is searched for by the MEGA collaboration at LAMPF [16] which stopped data-taking in 1995. The analysis of 16% of the data resulted in an upper limit of $4.2 \cdot 10^{-11}$ (90% C.L.) [18], just below the previous result. Since this subset already contains background it is doubtful that the final result will push the limit below 10^{-11}.

Given the stop rates required to reach a high sensitivity the main problem in a $\mu \to e\gamma$ search is the accidental background. Its level is roughly given by:

$$B_{acc} = R_\mu 2\delta x \frac{\alpha}{2\pi}(\delta y)^2(\ln(\delta y) + 7.3)(\delta z/2)^2 2\delta t \quad , \tag{12}$$

with R_μ: μ stop rate, x: e^- energy, y: γ energy, z: $\cos\theta_{e\gamma}$ and t: eγ time difference. x and y are normalized to 1. $\mu \to e\gamma$ events would be centered around $x = y = 1$, $z = t = 0$. The δ symbols denote single-sided cuts, i.e. $2\delta t$ corresponds to the time window.

The y dependence of B_{acc}, given by the photon energy distribution, is shown in Fig. 15. In Eq. 12 only $\mu^+ \to e^+\nu\overline{\nu}\gamma$ is taken into account. Depending on the setup annihilation in flight, pile-up events or cosmic rays might add to the background. Two parameter sets leading to B_{acc} levels below 10^{-14} are shown in Table 9. Correlated eγ pairs originate mainly in the decay $\mu^+ \to e^+\nu\overline{\nu}\gamma$ (see Fig. 16).

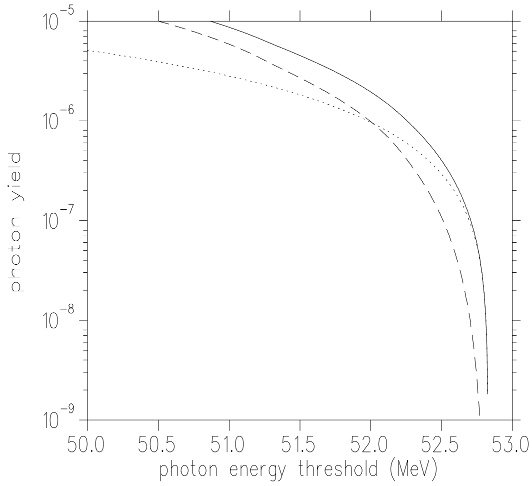

Figure 15: Photon yields v.s. energy threshold: dotted, from annihilation in flight in a 50 mg target; dashed, from radiative muon decay; solid, sum of the two.

Table 9: B_{acc} (Eq. 12) for different choices of stop rate and detector resolutions.

case	δx (%)	δy (%)	$\delta\theta_{e\gamma}$ (rad)	Δt (ns)	B_{acc}
1	1	2	0.01	0.3	2×10^{-15}
2	0.2	5	0.02	0.1	2×10^{-15}

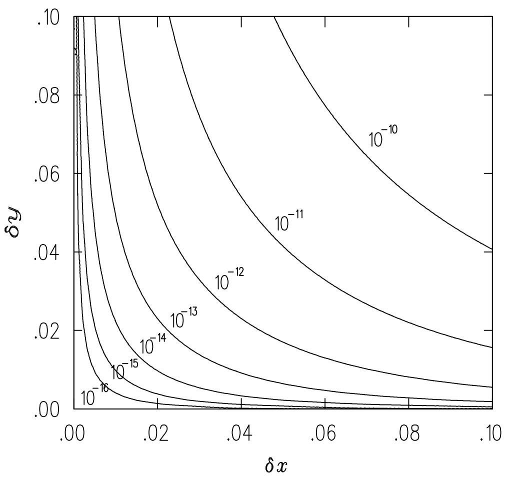

Figure 16: Prompt background contribution from $\mu^+ \rightarrow e^+\nu\overline{\nu}\gamma$ as a function of the windows on normalized positron and photon energies centered at the kinematic endpoint $x = y = 1$.

10.1 PSI letter of intent R-98-05.0

Recently a JINR-KEK-Pavia-Pisa-PSI-Roma-Swierk-Tbilisi-Tokyo-Waseda-Zurich collaboration submitted a letter of intent to *Search for the decay* $\mu^+ \to e^+\gamma$ *with a branching-ratio sensitivity of* 10^{-14} [17]. It is the aim to reach a single-event sensitivity below 10^{-14}, which would improve on the MEGA result by 2–3 orders of magnitude. Various alternative techniques, both for the positron spectrometer and for the photon calorimeter, are considered.

10.1.1 $\mu \to e\gamma$ setup with intermediate-focusing spectrometer

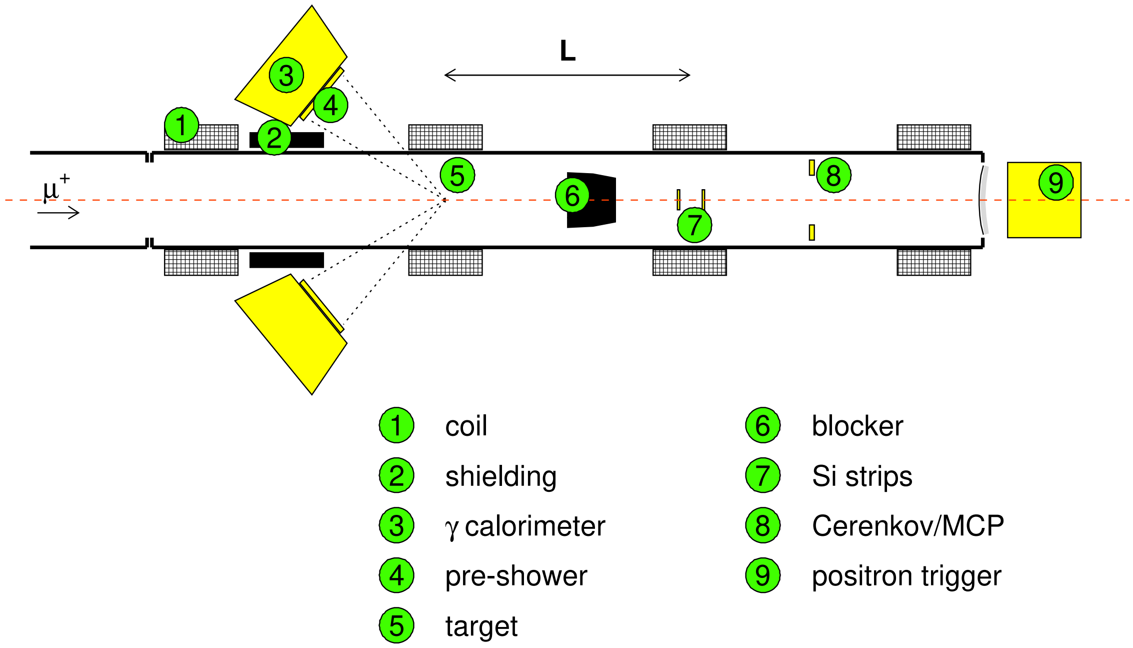

Figure 17: Intermediate-image spectrometer.

Figure 17 illustrates this scheme which combines an intermediate-focusing spectrometer with 5% momentum acceptance, 10% of 4π solid angle and 100 keV momentum resolution with a scintillator array, possibly of NaI(Tl) or GSO, preceeded by a sophisticated pre-shower detector for the ultimate position and timing resolution. The pre-shower detector would be made out of Cerium doped LSO or LuAP/YAP, and read through the front face similar to the xenon detector (see below).

10.1.2 $\mu \to e\gamma$ setup with liquid Xenon calorimeter

The scheme (see Fig. 18) makes use of a solenoidal spectrometer with a thin coil transparent to most photons at 50 MeV, which are detected in a liquid Xenon calorimeter ("mini-Kamiokande"). By measuring the spatial distribution of the scintillation light on all faces of the tank, it will be possible to reconstruct the interaction point of the photon

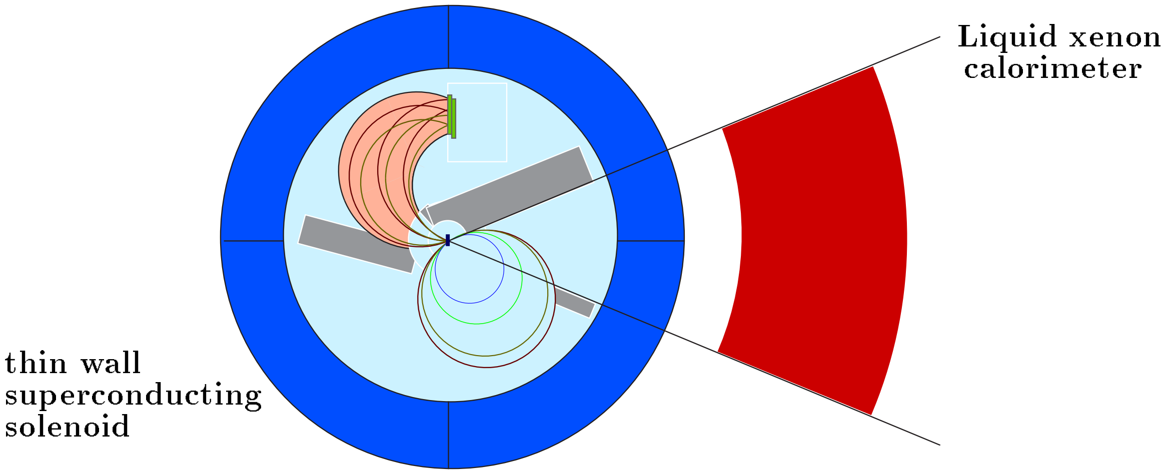

Figure 18: $\mu \to e\gamma$ setup with thin-wall superconducting coil and liquid Xenon gamma detector.

with a resolution of a few millimeter's. Liquid Xenon is a promising scintillator (density 3 g/cm^2, boiling point 165 K, radiation length 2.77 cm and decay time 45 ns (75%)) which is being studied at present.

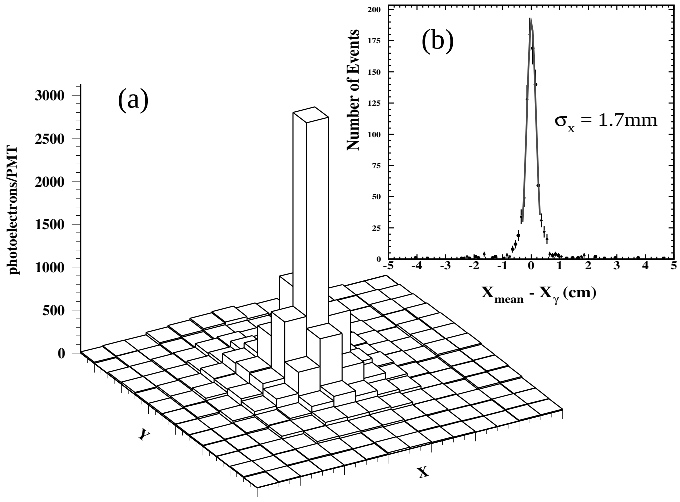

Figure 19: (a) Spatial distribution of light observed for a 50 MeV photon;
(b) Distribution of the position error using weighted-mean (results of a simulation).

A 50 MeV γ ray entering the liquid Xenon loses most of its energy near the entry point, typically within 2–10 cm from the surface, resulting in a distribution of the PMT outputs as shown in Fig. 19(a). According to the simulation the γ position, using the weighted mean of this distribution, can be determined to a precision of $\sigma \approx 1.7$ mm (Fig. 19(b)). The depth of the γ interaction point can be determined with a precision of $\sigma \approx 7$ mm.

11 Outlook

- Present observations are in perfect agreement with the predictions of the Standard Model, possibly with massive neutrinos as a minimal extension.
- Supersymmetry is the most popular extension to the model even if the number of free parameters increases considerably.
- Large regions of parameter space of minimal versions of the theory are already excluded by present experiments.
- Virtual processes, in particular L_i violating modes, may well give first hints of physics beyond the Standard Model, whether supersymmetric or not.
- Near-future experiments will push the sensitivities by three orders of magnitude.

References

[1] P. Fayet and S. Ferrara, Phys. Rep. 32 (1977) 249.

[2] G. Farrar and P. Fayet, Phys. Lett. B 76 (1978) 575.

[3] Hirsch *et al.*, Phys. Rev. D53 (1996) 1329.

[4] R. Barbieri, A. Strumia and Z. Berezhiani, Phys. Lett. B 407 (1997) 250.

[5] G. Bhattacharyya, invited talk at *Beyond the Desert*, Tegernsee, Germany, June 8-14 1997, `hep-ph/9709395`.

[6] SINDRUM Collaboration, U. Belgardt *et al.*, Nucl. Phys. B 299 (1988) 1.

[7] Super-Kamiokande Collaboration, M. Shiozawa *et al.*,

[8] M. Martinez, R. Miquel, L. Rolandi and R. Tenchini, CERN-EP/98-27, submitted to Review of Modern Physics

[9] J.Erler and D.M.Pierce, SLAC-PUB-7634

[10] L.J. Hall, V.A. Kostelecky and S. Raby, Nucl. Phys. B267 (1986) 415.

[11] R. Barbieri and L.J. Hall, Phys. Lett. 338B (1994) 212; R. Barbieri, L.J. Hall and A. Strumia, Nucl. Phys. B445 (1995) 219.

[12] J. Hiano, T. Moroi, K. Tobe, M. Yamaguchi and T. Yanagida, Phys. Lett. B391 (1997) 341.

[13] F. Herzog and K. Alder, Helv. Phys. Acta 53, 53 (1980).

[14] MECO Collaboration, W. Molzon spokesman, *A Search for* $\mu^- N \to E^- N$ *with Sensitivity Below* 10^{-16}, AGS proposal P940, 1997.

[15] MELC proposal, spokesmen R.M. Djilkibaev and V.M. Lobashev, INR - 786/92.

[16] MEGA, *Search for the Rare Decay* $\mu^+ \to e^+\gamma$, LAMPF proposal 969 (1985).

[17] *Search for the decay* $\mu^+ \to e^+\gamma$ *with a branching-ratio sensitivity of* 10^{-14}, PSI letter of intent R-98-05.0.

[18] R. Mischke, presented at the *International Workshop on JHF Science*, Tsukuba, Japan, March 3–7, 1998.